ELSEVIER

Journal of Photochemistry and Photobiology A: Chemistry 127 (1999) 21–30

Journal of Photochemistry and Photobiology A:Chemistry

www.elsevier.nl/locate/jphotochem

Triplet–triplet absorption of some organic molecules determined by picosecond laser excitation and time-delayed picosecond light continuum probing ☆

H. Gratz, A. Penzkofer *

Institut II — Experimentelle und Angewandte Physik, Universität Regensburg, D-93 040 Regensburg, Germany

Accepted 14 May 1999

Abstract

The triplet–triplet absorption cross-section spectra of eosin Y, erythrosin B, rose bengal and C_{70} are determined in the wavelength range from 390 to 1600 nm. The T_1 triplet state is populated by $S_1 \rightarrow T_1$ intersystem crossing after singlet state excitation with intense picosecond pump pulses (wavelength 527 nm, duration 6 ps). The triplet–triplet absorption is probed with picosecond spectral light continua passing the samples after excited singlet state relaxation (time delay 20 ns). Absolute triplet–triplet absorption cross-sections are obtained by numerical simulation of the absorption dynamics.

Keywords: Triplet–triplet absorption; Picosecond laser excitation; Eosin Y; Erythrosin B; Rose bengal; Fullerene molecule C_{70}

1. Introduction

The xanthene dyes eosin Y, erythrosin B, and rose bengal [1–3] as well as the fullerene molecule C_{70} [4] have large quantum yields of triplet formation. Laser excitation transfers part of the molecules to the triplet system and changes the absorption behavior of the molecules.

Triplet absorption data (peak extinction coefficients, ε_{max}, and peak wavelength positions, λ_{max}) of various molecules are collected in [5–7]. Methods of absolute triplet–triplet absorption cross-section determination are reviewed in [5]. A technique of spatial separation of triplet formation and triplet–triplet absorption detection in a flowing jet stream is reported in [8]. Absolute triplet–triplet absorption cross-section spectra, $\sigma_T(\lambda)$ over wide wavelength regions are scarcely found [8–14].

For eosin Y in methanol an absolute triplet–triplet absorption cross-section spectrum in the wavelength region from $\lambda = 400$ nm to $\lambda = 1000$ nm and at $\lambda = 308$ nm and $\lambda = 1054$ nm is reported in [15]. For erythrosin B in water at pH 9 a triplet–triplet absorption cross-section of $\sigma_T = (1 \pm 0.3) \times 10^{-16}$ cm^2 at $\lambda = 526$ nm is reported in [16]. In the wavelength region from 420 to 670 nm a triplet–triplet absorption cross-section spectrum for erythrosin in gelatin is displayed in [17]. At $\lambda = 525$ nm the triplet–triplet absorption cross-section is $\sigma_T = 4.6 \times 10^{-17}$ cm^2. For rose bengal in $5 \times l0^{-3}$ molar phosphate-buffered saline a triplet–triplet absorption cross-section spectrum in the region from 480 to 590 nm is given in [18]. At $\lambda = 530$ nm a value of $\sigma_T = 7.3 \times 10^{-17}$ cm^2 was determined. For C_{70} triplet–triplet absorption cross-section spectra are presented in [19,20] (solvent benzene, wavelength region 300–1620 nm), [21] (benzene, 435–700 nm), [22] (benzene and hexane, 300–700 nm), and [23] (benzene, 340–800 nm). Time resolved excited-state transmission spectra of C_{70} in toluene are given in [24] (wavelength range 550–1060 nm).

Here the triplet–triplet absorption cross-section spectra of eosin Y (disodium salt of 2′,4′,5′,7′-tetrabromofluorescein), erythrosin B (disodium salt of 2′,4′,5′,7′-tetraiodofluorescein), rose bengal (disodium salt of 3′,4′,5′,6′-tetrachloro-2,4,5,6-tetraiodofluorescein), and C_{70} are determined in the wavelength region from 390 to 1600 nm. The T_1-triplet state is populated by picosecond pump pulse singlet–singlet state absorption and subsequent intersystem crossing. The triplet–triplet absorption is probed after excited singlet population relaxation by time delayed picosecond light continuum transmission measurement. The absorption and relaxation dynamics is described theoretically and analyzed numerically to extract absolute triplet–triplet absorption cross-section spectra, $\sigma_T(\lambda)$. The sensitive dependence of

☆ This paper is dedicated to Professor K.-H. Drexhage on the occasion of his emeritation.

* Corresponding author. Fax: +49-941-943-2754

E-mail address: alfons.penzkofer@physik.uni-regensburg.de (A. Penzkofer)

1010-6030/99/$ – see front matter
PII: S1010-6030(99)00152-5

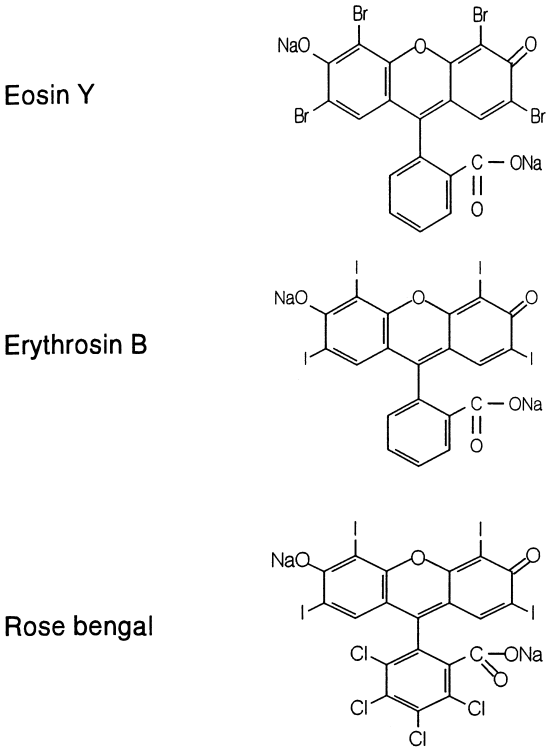

Fig. 1. Structural formulae of investigated xanthene dyes.

$\sigma_T(\lambda)$ on the quantum yield of triplet formation, ϕ_T in the region of strong ground-state singlet absorption is used to determine ϕ_T. The applied technique of single picosecond pulse excitation avoids the complications of triplet–singlet back intersystem crossing by pump pulse triplet–triplet excitation when the excitation pulse becomes comparable to or longer than the fluorescence lifetime [25–27].

2. Experimental

The structural formulae of the xanthene dyes eosin Y, erythrosin B, and rose bengal are displayed in Fig. 1. They were dissolved in methanol. In the long-wavelength region ($\lambda > 1430$ nm) methanol was replaced by deuterated methanol (CD_4O) because methanol becomes absorbing. The fullerene C_{70} was dissolved in toluene. All dyes and solvents were purchased from Aldrich. They are used without further purification.

The experiments are carried out with a mode-locked Nd : phosphate glass laser system [28] using a picosecond pump and probe technique. The experimental setup is shown in Fig. 2. A mode-locked laser oscillator generates a train of picosecond pulses. A single pulse is selected with a laser-triggered Kerr shutter and amplified in a Nd : phosphate glass laser amplifier (wavelength $\lambda_L = 1054$ nm, energy $W_L \approx 3$ mJ, duration $\Delta t_L = 6$ ps). In a CDA crystal [29] part of the fundamental laser energy is frequency doubled ($\lambda_P = 527$ nm, $W_P \approx 1$ mJ). The second harmonic light is separated from the fundamental light by a harmonic beam splitter, HBS. The second harmonic pulses are used as pump pulses to excite the sample, S, to the triplet state, T_1, via ground-state singlet–singlet absorption and subsequent intersystem-crossing. The pump pulses are focused to the sample by lens L1. The input pump pulse peak energy density, w_{0P}, at the sample is determined by energy transmission measurement through a cell filled with rhodamine 6G in ethanol (slow saturable absorber) [30] with the photodetectors PD1 and PD2. The pump pulse energy transmission through the samples is measured with the photodetectors PD1 and PD3.

The fundamental laser pulse ($\lambda_L = 1054$ nm) passes through an optical delay line, DL (temporal delay $t_d \approx 20$ ns) and is then focused (lens L2) into a heavy water sample (length 5 cm) to generate a picosecond light continuum [31,32]. The light continuum is collimated with lens L3 and focused to the sample, S, with lens L4. The remaining fundamental light is blocked with a mirror, M. The beam diameters of the pump and probe pulses are measured and the spatial overlap of the pump and probe pulses is controlled with a camera. The spectral distributions of the incident and transmitted light continua are registered with two spectrometer–diodearray systems SP1, DAl and SP2, DA2. The transmission spectra are obtained by dividing the output spectra through the input spectra and calibrating the detection systems by using the solvents as samples. Silicon diode arrays are used in the wavelength region from 390 to 1100 nm, while in the wavelength region from 1100 to 1600 nm two InGaAs photodiode arrays were used (model XMCD-256-IR-SU arrays from Polytec, Waldbronn, Germany).

The pump pulse excited-state absorption cross-section, $\sigma_{ex,L}$, is determined by pump pulse transmission measurement (photodetectors PD1 and PD3) and numerical simulation of the intensity dependent pump pulse absorption.

The pump-pulse photodegradation of the dyes is measured by repeated single-shot excitation of small-volume samples (number of shots, m_P). The inner diameter of the cell was $d_A = 2r_A = 1$ mm and the $1/e$-beam diameter, $d_P = 2r_P$, was made equal to the inner cell diameter. The pump pulse peak intensity, $I_{0P,i}$ ($i = 1$ to m_P), of the single shots was measured and the mean value, $\bar{I}_{0P} = \sum_{i=1}^{m_P} I_{0P,i}/m_P$ was determined. The initial small-signal transmission, $T_i(\lambda)$ and the final small-signal transmission, $T_f(\lambda)$, after m_P laser shots (m_P of the order of 30) was determined by measuring the transmission of picosecond light continua before and after repeated pump pulse excitation. The fraction of photodegraded molecules, N_D/N_0, per laser shot of average spatial peak intensity, $\bar{I}_P = \int_0^{T_A} r\bar{I}_{0P}(r)dr/r_A^2$, is given by

$$\frac{N_D}{N_0} = \frac{1}{m_P}\left(1 - \frac{\ln(T_f)}{\ln(T_i)}\right). \quad (1)$$

The quantum yield of photodegradation, ϕ_D, is extracted from $N_D(\bar{I}_P)/N_0$ by numerical simulation (see below).

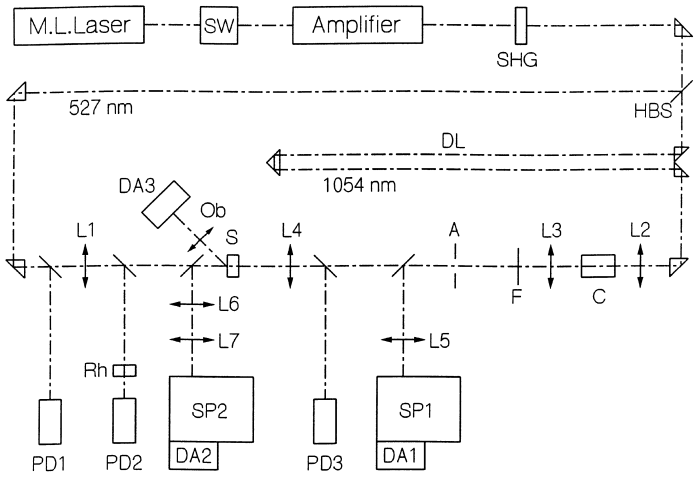

Fig. 2. Experimental setup. M.L.Laser, mode-locked Nd : phosphate glass laser. SW, Kerr shutter [60]. Amplifier, Nd : phosphate glass laser amplifier. SHG, CDA crystal for second harmonic generation. HBS, harmonic beam splitter. DL, optical delay line. L1–L7, lenses. S, sample, C, D_2O sample for light continuum generation. F, mirror for fundamental laser blocking. A, aperture. PD1–PD3, photodiodes. SP1, SP2, grating spectrometers. DA1–DA3, diode-array detectors. Ob, camera objective.

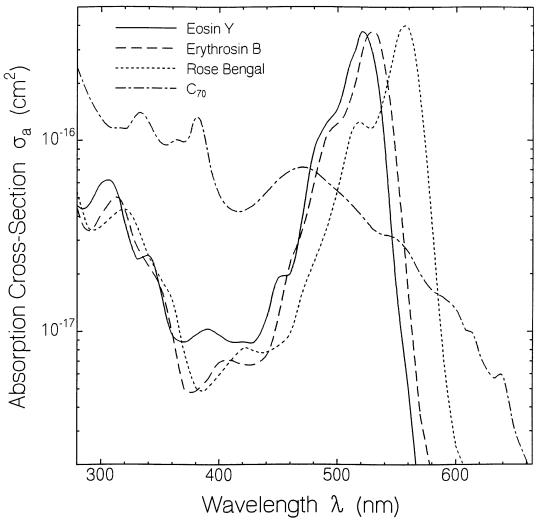

Fig. 3. Absorption cross-section spectra of eosin Y in methanol, erythrosin B in methanol, rose bengal in methanol, and C_{70} in toluene at room temperature.

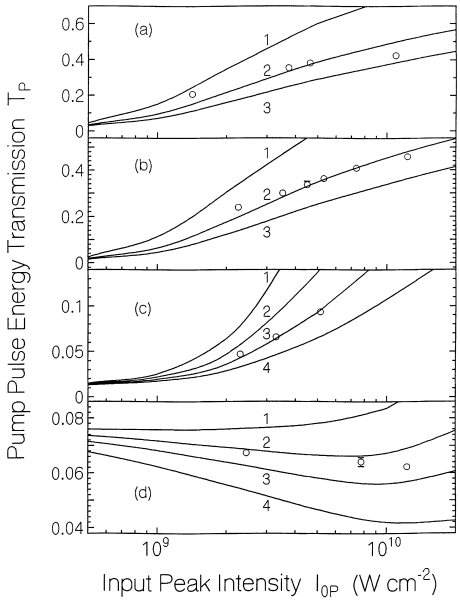

Fig. 4. Intensity dependent energy transmission of pump pulses through samples. Circles are measured and curves are calculated using parameters listed in Table 1. (a) Eosin Y in methanol. Small-signal transmission $T_0 = 0.0082$. The curves belong to (l) $\sigma_{ex,P} = 0$, (2) 3×10^{-17} cm^2, (3) 5×10^{-17} cm^2. (b) Erythrosin B in methanol. $T_0 = 0.0035$. (1) $\sigma_{ex,P} = 0$. (2) 3×10^{-17} cm^2, (3) 5×10^{-17} cm^2. (c) Rose bengal in methanol, $T_0 = 0.0094$. (1) $\sigma_{ex,P} = 0$, (2) 2×10^{-17} cm^2, (3) 3×10^{-17} cm^2, (4) 4×10^{-17} cm^2. (d) C_{70} in Toluene. $T_0 = 0.0747$. (1) $\sigma_{ex,P} = 4 \times 10^{-17}$ cm^2, (2) 5×10^{-17} cm^2, (3) 6×10^{-17} cm^2, (4) 8×10^{-17} cm^2.

3. Results

The ground state absorption cross-section spectra of the investigated xanthene dye and C_{70} fullerene solutions are displayed in Fig. 3. The spectra were obtained by transmission measurements with a spectrophotometer (Beckman ACTA M IV).

The nonlinear pump pulse transmission results for excited-state absorption determination are shown in Fig. 4 (circles). A saturable absorption [33] (decrease of absorption with rising pump pulse intensity) is observed for eosin Y, erythrosin B, and rose bengal, while a reverse saturable absorption [34] (increase of absorption with pump pulse intensity) occurs for C_{70} [35,36]. Below, excited-state absorption cross-sections, $\sigma_{ex,P}$, are extracted by comparing the experimental energy transmissions with numerical simulations. The fractions of degraded molecules, N_D/N_0, at fixed, spatially averaged pump pulse peak intensities, $\bar{I}_P$ are displayed by circles in Fig. 5 for eosin Y (a), erythrosin B (b), and rose bengal (c). Eq. (1) was used to calculate N_D/N_0 from measured transmission changes. Typically 1% of the molecules was degraded per laser shot (input pump

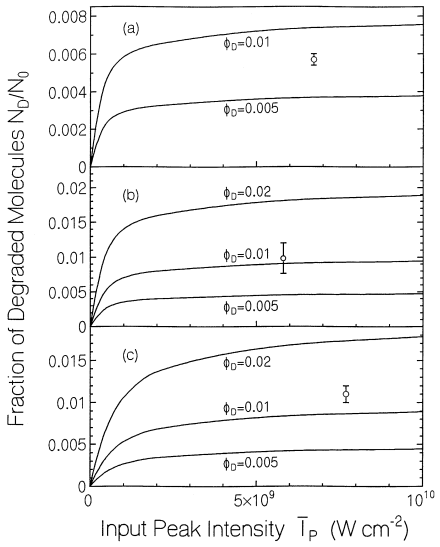

Fig. 5. Fraction of degraded molecules, N_D/N_0, vs. spatially averaged input pump pulse peak intensity, $\bar{I}_P = 0.7\,\bar{I}_{0P}$ Circles are determined from measurements using Eq. (1). Curves are calculated for various quantum yields of photodegradation, ϕ_D. Sample thickness $\ell = 1$ mm. (a) Eosin Y. Initial small signal transmission $T_i(521\,\text{nm}) = 0.023$. Final small-signal transmission $T_f(521\,\text{nm}) = 0.054$. Number of laser shots $m_P = 40$. Average pump pulse peak intensity $\bar{I}_{0P} = 9.6\times10^9\,\text{W cm}^{-2}$. (b) Erythrosin B. $T_i(527\,\text{nm}) = 0.024$. $T_f(527\,\text{nm}) = 0.05$. $m_P = 20$. $\bar{I}_{0P} = 8.3\times10^9\,\text{W cm}^{-2}$. (c) Rose bengal. $T_i(556\,\text{nm}) = 0.14$. $T_f(556\,\text{nm}) = 0.42$. $m_P = 50$. $\bar{I}_{0P} = 1.1\times10^{10}\,\text{W cm}^{-2}$.

energy density $w_P \approx 50\,\text{mJ cm}^{-2}$). For C_{70} in toluene no change in transmission was observed after 50 laser shots of peak intensity $\bar{I}_{0P} = 1.4\times10^{10}\,\text{W cm}^{-2}$. The photodegradation of C_{70} is negligibly small under our experimental conditions. The quantum yield of photodegradation, ϕ_D, is derived from the fraction of degraded molecules, N_D/N_0, by numerical simulation (see below).

The results of the triplet–triplet absorption measurements are shown in Figs. 6–9. The transmission ratio, $T_{pr}(\lambda,I_{0P})/T_{pr}(\lambda,0)$, of picosecond light continuum transmission in the case of pump pulse excitation, $T_{pr}(\lambda,I_{0P})$, to the case without pump pulse excitation, $T_{pr}(\lambda,0)$, is displayed. The probe pulse continuum is delayed in time relative to the pump pulse excitation by $t_d = 20$ ns in order to allow complete S_1-state depopulation by relaxation to the T_1-triplet state (intersystem crossing) and the S_0-singlet state (internal conversion and fluorescence emission). The wavelength range from 390 to 1600 nm is covered by six different spectrometer and filter settings. The curve segments with the corresponding small signal transmissions, T_0, and the mean pump pulse peak intensities, $\bar{I}_{0P}$ are shown in the figures. Each curve segment was obtained by averaging over approximately 10 laser shots.

In the ground-state-absorption-free long wavelength region the transmission ratio $T_{pr}(\lambda,I_{0P})/T_{pr}(\lambda,0)$ is equal to the triplet–triplet transmission $T_{T1}(\lambda,I_{0P})$. In the ground-state absorption region $T_{pr}(\lambda,I_{0P})$ is composed of T_1-triplet–triplet absorption and residual ground-state absorption, while $T_{pr}(\lambda,0)$ is the initial small signal ground-state absorption

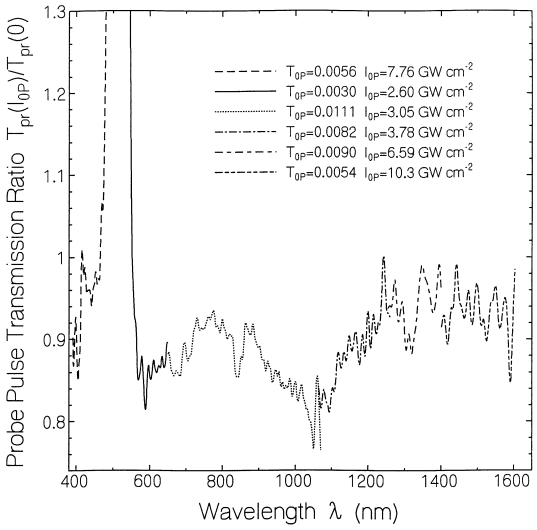

Fig. 6. Probe pulse transmission ratio, $T_{pr}(\lambda, I_{0P})/T_{pr}(\lambda, 0)$ for eosin Y in methanol. Sample length $\ell = 1$ mm. The small-signal transmissions, T_{0P}, at the laser wavelength, λ_P, and the pump pulse peak intensities, I_{0P}, are indicated. Pump beam diameter at sample $\Delta d_P = 2[\ln(2)]^{1/2}\,r_p \approx 0.85$ mm. Probe beam diameter $\Delta d_{pr} \approx 0.25$ mm.

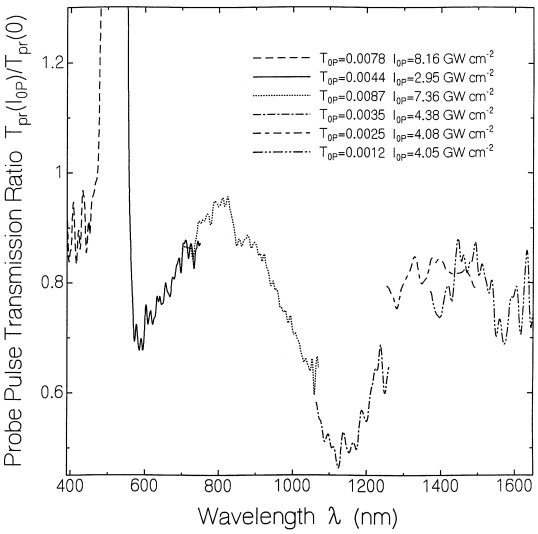

Fig. 7. Probe pulse transmission ratio, $T_{pr}(\lambda, I_{0P})/T_{pr}(\lambda,0)$, for erythrosin B in methanol, $\ell = 1$ mm. T_{0P} and I_{0P} of the curve segments are given by the legend. $\Delta d_P \approx 0.85$ mm. $\Delta d_{pr} \approx 0.25$ mm.

($T_{pr}(\lambda, 0) = \exp[-N_0\sigma_a(\lambda)\ell]$). A transmission ratio of $T_{pr}(\lambda,I_{0P})/T_{pr}(\lambda,0) > 1$ indicates that the T_1 triplet–triplet absorption cross-section, $\sigma_T(\lambda)$, is less than the S_0 singlet–singlet absorption cross-section $\sigma_a(\lambda)$. A numerical procedure to determine $\sigma_T(\lambda)$ from the transmission ratio, $T_{pr}(\lambda,I_{0P})/T_{pr}(\lambda,0)$, is given below.

4. Theoretical description

The pump-pulse absorption, probe-pulse absorption, molecular relaxation, and photo-degradation are analyzed using the energy level system of Fig. 10.

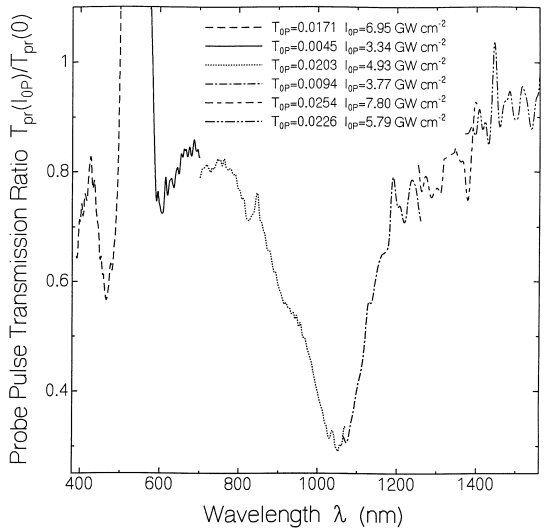

Fig. 8. Probe pulse transmission ratio, $T_{pr}(\lambda,I_{0P})/T_{pr}(\lambda,0)$, for rose bengal in methanol, $\ell = 1$ mm. T_{0P} and I_{0P} of the curve segments are given by the legend. $\Delta d_P \approx 0.85$ mm. $\Delta d_{pr} \approx 0.25$ mm.

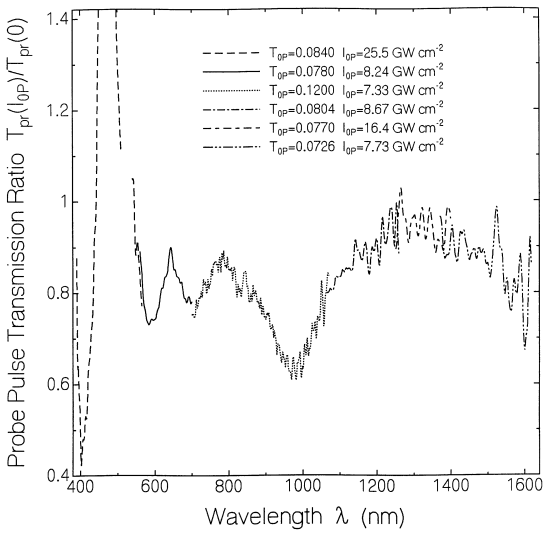

Fig. 9. Probe pulse transmission ratio, $T_{pr}(\lambda,I_{0P})/T_{pr}(\lambda,0)$ for C_{70} in toluene, $\ell = 1$ mm. T_{0P} and I_{0P} of the curve segments are given by the legend. $\Delta d_P \approx 0.7$ mm. $\Delta d_{pr} \approx 0.25$ mm.

The pump pulses excite molecules from the ground-state S_0 (level 1) to a vibronic Franck-Condon state $2'$ in the S_1-band. From there the molecules relax to a temporal thermal equilibrium state 2 in the S_1-band with a relaxation time τ_{FC}. Starting from the S_1-band there occurs pump pulse excited-state absorption (cross-section, $\sigma_{ex,P}$) to a higher lying singlet-state S_n. Higher excited molecules in the singlet system relax back to the S_1-band with a time constant τ_{ex}. The molecules in the S_1 band relax to the ground-state (radiative relaxation with fluorescence quantum yield ϕ_F, and internal conversion), to the T_1-triplet state (intersystem crossing, quantum efficiency ϕ_T) and photo-degrade (quantum yield of degradation ϕ_D).

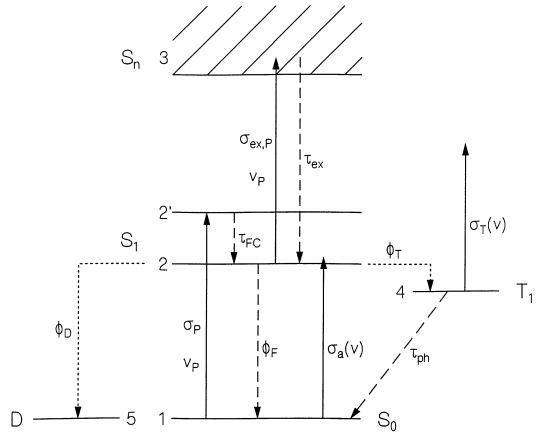

Fig. 10. Energy level diagram applied to numerical analysis of absorption dynamics.

At a delay time, t_d, long compared to the S_1-state lifetime, τ_{S_1} , (fluorescence lifetime τ_F) and short compared to the triplet T_1-state life time, τ_{T_1}, (phosphorescence lifetime τ_{ph}), a probe pulse is absorbed by residual ground state absorption (cross-section $\sigma_a(\nu)$) and T_1-triplet–triplet absorption (cross-section $\sigma_T(\nu)$). The probe pulse energy density should be small compared to the S_0 and T_1saturation energy densities [33] in order to avoid population changes by the transmission probing. The slow saturable absorber (pulse duration, Δtp (FWHM), short compared to absorption recovery time $\tau_A = \tau_F$) saturation energy at the pump laser frequency, ν_P, is given by [37]

$$I_{sat,S} = \frac{h\nu_P}{\sigma_P \Delta t_P}, \tag{2}$$

where h is the Planck constant, and $\sigma_P = \sigma_a(\nu_P)$ is the ground-state absorption cross-section at the pump laser frequency ν_P.

The dynamics of the level population number densities, N_i (r,z',t',θ), $i = 1$–5, by pump pulse, $I_P(r,z',t')$, absorption is described by the following equation system [38]

$$\frac{\partial N_1}{\partial t'} = -\frac{3\sigma_P \cos^2(\theta)}{h\nu_P}(N_1 - N_{2'})I_P + (1-\phi_T-\phi_D)\frac{N_2+N_{2'}}{\tau_{S_1}} + \frac{N_4}{\tau_{ph}} - \frac{N_1-\bar{N}_1}{\tau_{or}}, \tag{3}$$

$$\frac{\partial N_{2'}}{\partial t'} = \frac{3\sigma_P \cos^2(\theta)}{h\nu_P}(N_1 - N_{2'})I_P - \frac{N_{2'}-N_{2',th}}{\tau_{FC}} - \frac{N_{2'}}{\tau_{S_1}} - \frac{3\sigma_{ex,P}\cos^2(\theta)}{h\nu_P}\left(N_{2'} - \frac{N_{2'}}{N_2+N_{2'}}N_3\right)I_P - \frac{N_{2'}-\bar{N}_{2'}}{\tau_{or}}, \tag{4}$$

$$\frac{\partial N_2}{\partial t'} = \frac{N_{2'}}{\tau_{FC}} - \frac{3\sigma_{ex,P}\cos^2(\theta)}{h\nu_P}\left(N_2 - \frac{N_2}{N_2+N_{2'}}N_3\right)I_P - \frac{N_2}{\tau_{S_1}} + \frac{N_3}{\tau_{ex}} - \frac{N_2-\bar{N}_2}{\tau_{or}}, \tag{5}$$

$$\frac{\partial N_3}{\partial t'} = \frac{3\sigma_{ex,P}\cos^2(\theta)}{h\nu_P}(N_2 + N_{2'} - N_3)I_P - \frac{N_3}{\tau_{ex}} - \frac{N_3 - \bar{N}_3}{\tau_{or}}, \quad (6)$$

$$\frac{\partial N_4}{\partial t'} = \frac{\phi_T}{\tau_{S_1}}(N_2 + N_{2'}) - \frac{N_4}{\tau_{ph}} - \frac{N_4 - \bar{N}_4}{\tau_{or}}, \quad (7)$$

$$\frac{\partial N_5}{\partial t'} = \frac{\phi_D}{\tau_{S_1}}(N_2 + N_{2'}), \quad (8)$$

$$\frac{\partial I_P}{\partial z'} = -3\sigma_P I_P \int_0^{\pi/2}(N_2 - N_{2'})\cos^2(\theta)\sin(\theta)\mathrm{d}\theta - 3\sigma_{ex} I_P \int_0^{\pi/2}(N_2 + N_{2'} - N_3)\cos^2(\theta)\sin(\theta)\mathrm{d}\theta - \alpha^{(2)} I_P^2, \quad (9)$$

$$\bar{N}_i = \int_0^{\pi/2} N_i(\theta)\sin(\theta)\mathrm{d}\theta \quad i = 1, 2, 2', 3, 4, 5. \quad (10)$$

$$N_{2',th} = (N_2 + N_{2'})\exp\left(-\frac{h\nu_{22'}}{k_B\vartheta}\right). \quad (11)$$

The moving frame transformation $t' = t - nz/c_0$ and $z' = z$ is used, where t is the time, z the propagation coordinate, n the refractive index, and c_0 the vacuum light velocity. θ is the angle between the molecular transition dipole moment and the polarization direction of the pump laser [39]. τ_{or} is the reorientation time of the transition dipole moment. $\bar{N}_i$ is the orientation averaged population of level i. $N_{2',th}$ is the thermal population of level $2'$. $h\nu_{22'} = hc_0\tilde{\nu}_{22'}$ is the energy difference between level $2'$ and 2. k_B is the Boltzmann constant, and ϑ the temperature. The term $-\alpha^{(2)} I_P^2$ in Eq. (9) takes care of two-photon absorption of the solvent. $\alpha^{(2)}$ is the two-photon absorption coefficient ($\alpha^{(2)} = 2 \times 10^{-10}$ cm W^{-1} for toluene [36], $\alpha^{(2)} \approx 0$ for methanol at $\lambda_P = 527$ nm).

The initial conditions are $N_1(r,t' = -\infty,z',\theta) = N_0$, $N_2(r,t' = -\infty,z',\theta) = N_{2'}$, $(r,t' = -\infty,z',\theta) = N_3(r,t' = -\infty,z',\theta) = N_4(r, t' = -\infty,z',\theta) = N_5(r,t' = -\infty,z',\theta) = 0$, and $I_P(r,t',z' = 0) = I_{0P}\exp(-r^2/r_P^2)\exp(-t'^2/t_P^2)$. r is the radial coordinate, r_P the 1/e-intensity pump beam radius.

The pump pulse energy transmission is

$$T_P = \frac{\int_0^\infty r\mathrm{d}r\int_{-\infty}^{\infty}\mathrm{d}t' I_P(r,\ell,t')}{\int_0^\infty r\mathrm{d}r\int_{-\infty}^{\infty}\mathrm{d}t' I_P(r,0,t')}, \quad (12)$$

where ℓ is the sample length.

At the time, t_d, of probing, the level populations have relaxed to

$$N_1(r,z',t_d,\theta) = \bar{N}_1(r,z,t_d) = \bar{N}_1(r,z,t_e) + [\bar{N}_2(r,z,t_e) + \bar{N}_{2'}(r,z,t_e) + \bar{N}_3(r,z,t_e)](1 - \phi_T - \phi_D), \quad (13)$$

$$N_4(r,z',t_d,\theta) = \bar{N}_4(r,z,t_d) = \bar{N}_4(r,z,t_e) + \phi_T[\bar{N}_2(r,z,t_e) + \bar{N}_{2'}(r,z,t_e) + \bar{N}_3(r,z,t_e)], \quad (14)$$

$$N_5(r,z',t_d,\theta) = \bar{N}_5(r,z,t_d) = \bar{N}_5(r,z,t_e) + \phi_D[\bar{N}_2(r,z,t_e) + \bar{N}_{2'}(r,z,t_e) + \bar{N}_3(r,z,t_e)], \quad (15)$$

and $N_2(r,z',t_d,\theta) = N_{2'}(r,z',t_d,\theta) = N_3(r,z',t_d,\theta) = 0$. t_e is the time position at the end of the pump pulse ($t_e = 5\ t_P$ is used in calculations).

The length averaged population number densities are

$$\mathcal{N}_i(r,t_d) = \frac{1}{\ell}\int_0^\ell \bar{N}_i(r,z,t_d)\mathrm{d}z \quad i = 1, 4, 5 \quad (16)$$

The probe pulse transmission, $T_{pr}(\lambda,I_{0P})$, at wavelength λ after pump pulse absorption (delay time t_d) is given by

$$T_{pr}(\lambda, I_{0P}) = \frac{\int_0^\infty \exp(-r^2/r_{pr}^2)\exp\{-[\sigma_a(\lambda)\mathcal{N}_1(r,t_d) + \sigma_T(\lambda)\mathcal{N}_4(r,t_d)]\ell\}\,\mathrm{d}r}{\int_0^\infty r\exp(-r^2/r_{pr}^2)\mathrm{d}r}, \quad (17)$$

where r_{pr} is the l/e-intensity probe beam radius. The probe pulse transmission without pump pulse excitation is

$$T_{pr}(\lambda, 0) = \exp[-\sigma_a(\lambda)N_0\ell] \quad (18)$$

5. Data analysis

The parameters of the investigated xanthene dyes and of C_{70} which are used in the numerical data analysis are listed in Table 1 and in the figure captions. The excited-state absorption cross-sections, $\sigma_{ex,P}$, at the pump pulse wavelength are determined by fitting Eq. (12) to the experimental pump-pulse energy transmission measurements (Fig. 4). The quantum yields of photodegradation, ϕ_D, are found by fitting $N_D/N_0 = \mathcal{N}_5(r = 0, t_d, I_{0P} = \bar{I}_P)/N_0$ to the experimentally determined fractions of degraded molecules per laser shot (Fig. 5). The triplet–triplet absorption cross-section spectra, $\sigma_T(\lambda)$ are obtained by fitting the calculated probe pulse transmission ratios (Eqs. (17) and (18)) to the experimental probe pulse transmission ratios (Figs. 6–9).

In Fig. 4(a–d) the calculated pump pulse energy transmissions, T_P, versus input peak intensity, I_{0P}, are shown for several excited state absorption cross-sections, $\sigma_{ex,P}$. The best fit to the experimental T_P-values determines the $\sigma_{ex,P}$-values of the samples. The obtained $\sigma_{ex,P}$-data are listed in Table 1.

In Fig. 5(a–c) calculated fractions of degraded molecules, $N_D/N_0 = \mathcal{N}_5(r = 0, t_d, I_{0P} = \bar{I}_P)/N_0$ versus input peak intensity, $\bar{I}_P$ are plotted for several quantum yields of photodegradation, ϕ_D. The best fitting ϕ_D-values to the experimentally determined N_D/N_0-fractions are listed in Table 1.

The extracted $\sigma_T(\lambda)$-spectra from the measured probe pulse transmission ratios, $T_{pr}(\lambda, I_{0P})/T_{pr}(\lambda, 0)$ (Figs. 6–9) are drawn in Figs. 11–14.

In the region of the strong S_0–S_1 ground-state absorption the σ_T-values are quite sensitive to $\mathcal{N}_1(r, t_d)$ and $\mathcal{N}_4(r, t_d)$ which depend on I_{0P}, ϕ_T, and $\sigma_{ex,P}$. High pump pulse peak intensities, $I_{0P} \gg I_{sat,S}$ (Eq. (2)), and small probe beam to pump

Table 1
Spectroscopic parameters of investigated samples at room temperature

Parameter	Eosin Y in methanol	Erythrosin B in methanol	Rose bengal in methanol	C_{70} in toluene	Comments
σ_P (cm^2)	3.2×10^{-16}	3.6×10^{-16}	1.16×10^{-16}	3.6×10^{-17}	Fig. 3
$\sigma_{ex,P}$ (cm^2)	$(2.9 \pm 0.3) \times 10^{-17}$	$(3.0 \pm 0.3) \times 10^{-17}$	$(2.9 \pm 0.4) \times 10^{-17}$	$(5.3 \pm 0.5) \times 10^{-17}$	Fig. 4
λ_{S1}[a] (nm)	533.8	545.5	568.5	638	
$\tilde{\nu}_{2,2'}$ (cm^{-1})	242	643	1385	3300	$\tilde{\nu}_{22'} = \lambda_P^{-1} - \lambda_{S_1}^{-1}$
τ_{S1} (ns)	2.0 [38]	0.53 [51]	0.59 [51]	0.65 [36]	
τ_{FC} (ps)	0.5	0.5	0.5	0.5	assumed [61]
τ_{Sn} (fs)	60[b]	60[b]	60[b]	240 [36]	
τ_{or} (ps)	330 [62]	200 [54]	150 [54]	23[c]	
ϕ_T	0.56 [15]	0.90 ± 0.03[d]	0.90 ± 0.04[d]	1.0 [36]	
ϕ_D	0.0077 ± 0.001	0.0108 ± 0.002	0.0125 ± 0.002	0 ± 0.003	Fig. 5
$\phi_{sat,S}$ ($W\,cm^{-2}$)	2×10^8	1.7×10^8	5.4×10^8	1.7×10^9	Eq. (2)

[a] λ_{S1} is wavelength of pure electronic S_0–S_1 transition.
[b] Assumed [63].
[c] Calculated by using the relation $\tau_{or} = \eta V_m / k_B \vartheta$ [54], where $\eta = 5.9 \times 10^{-3}$ Pas [64] is the viscosity of toluene, $V_m = 1.56 \times 10^{-22}$ cm^3 is the volume of C_{70} ([4] p. 67), k_B the Boltzman constant and $\vartheta = 293$ K is the room temperature.
[d] This work.

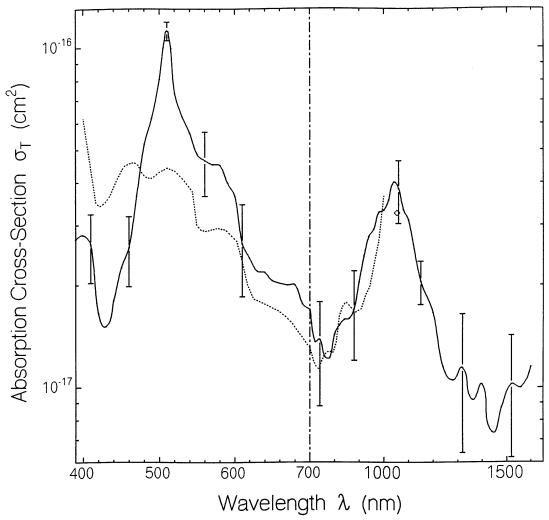

Fig. 11. Triplet–triplet absorption cross-section spectra of eosin Y in methanol for $\lambda < 1430$ nm and in deuterated methanol for $\lambda > 1430$ nm. Solid curve, calculated $\sigma_T(\lambda)$ by use of transmission data (Fig. 6). Dotted curve and diamond, redrawn from [15].

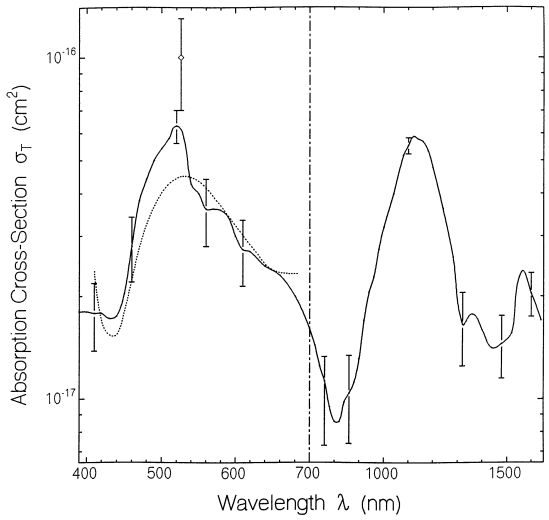

Fig. 12. Triplet–triplet absorption cross-section spectra of erythrosin B. Solid curve, calculated $\sigma_T(\lambda)$ by use of transmission data (Fig. 7). Solvent is methanol for $\lambda < 1430$ nm and deuterated methanol for $\lambda > 1430$ nm. Dotted curve, redrawn from [17]. It belongs to erythrosin in gelatin. Diamond, value is taken from [16]. It belongs to erythrosin B in water at pH 9.

beam ratios, r_{pr}/r_P are favorable, since then the triplet system population approaches $N_T/N_0 \approx \phi_T$ and becomes insensitive to I_{0P} and $\sigma_{ex,P}$. Using a smaller ϕ_T value than the true quantum yield of triplet formation would result in a dip in the σ_T-spectra at the region of maximum ground-state absorption. A smooth continuation of the triplet–triplet absorption spectra through the peak absorption region allows an accurate ϕ_T-determination. The best-fitting ϕ_T-values are listed in Table 1.

6. Discussion

The T_1-state triplet–triplet absorption cross-section spectra of eosin Y, erythrosin B, rose bengal, and C_{70} presented in Figs. 11–14 were determined by picosecond pulse excitation and 20 ns delayed picosecond light continuum probing. The picosecond pulse excitation and triplet absorption probing shortly after singlet excited-state relaxation makes it very likely that the spectra are due to true T_1–T_n triplet–triplet absorption and are not modified by transient photo-product formation like semi-oxidized and semi-reduced radical production in the triplet state within the phosphorescence life time [40–43].

The triplet–triplet absorption spectra extend over the whole investigated wavelength region from 1600 to 390 nm. The triplet–triplet absorption may extend to even longer wavelengths. This longer wavelength region was not accessible with the present picosecond continuum probing and InGaAs diode-array detection. The ground state absorp-

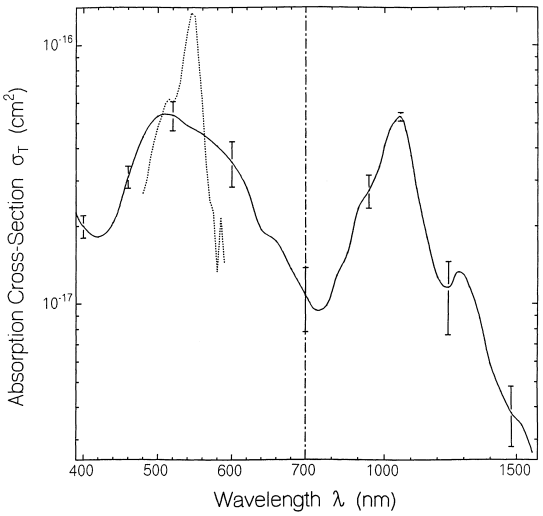

Fig. 13. Triplet–triplet absorption cross-section spectra of rose bengal. Solid curve, calculated form transmission data (Fig. 8). Solvent is methanol for $\lambda < 1430$ nm and deuterated methanol for $\lambda > 1430$ nm. Dotted curve, presents absorption cross-section spectrum of rose bengal in 5×10^{-3} molar phosphate-buffered saline. It is redrawn from [18].

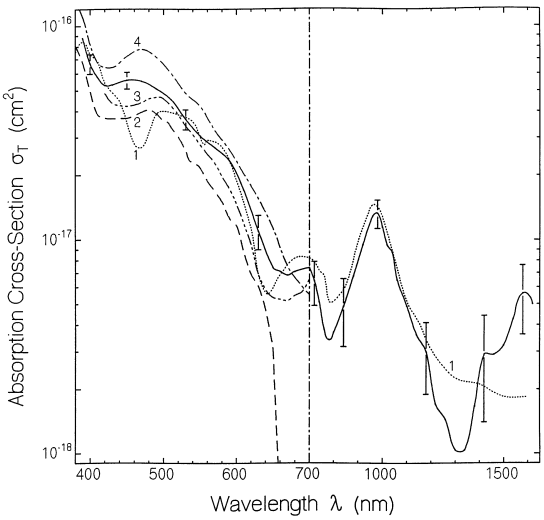

Fig. 14. Triplet–triplet absorption cross-section spectra of C_{70}. Solid curve, calculated form transmission data (Fig. 9). Solvent is toluene. The other curves present triplet–triplet absorption cross-section spectra of C_{70} in benzene. These curves are taken from the literature. Dotted curve 1, taken from [19]. Dashed curve 2, taken from [23]. Dash-triple-dotted curve 3, taken from [21]. Dashed-dotted curve 4, taken from [22].

tion cross-section spectra of Fig. 3 indicate S_2–S_1 energy spacings of $\tilde{\nu}_{S_2S_1}$(eosin Y) $\approx 4800\,\mathrm{cm}^{-1}$, $\tilde{\nu}_{S_2S_1}$(erythrosin B) $\approx 5700\,\mathrm{cm}^{-1}$, $\tilde{\nu}_{S_2S_1}$(rose bengal) $\approx 5600\,\mathrm{cm}^{-1}$ (energy spacings would be smaller if the S_2-state would be hidden within the S_1-absorption band), and $\tilde{\nu}_{S_2S_1}(C_{70}) \approx 750\,\mathrm{cm}^{-1}$. Similar energy spacings are expected between the T_2 and T_1 states. These T_2–T_1 energy separations are small compared to the T_1–S_0 energy separations which are determined by the wavelength positions of phosphorescence onset: $\tilde{\nu}_{T_1S_0}$(eosin Y) $\approx 15{,}900\,\mathrm{cm}^{-1}$ [44,45], $\tilde{\nu}_{T_1S_0}$(erythrosin B) = 15,800 cm^{-1} [46], $\tilde{\nu}_{T_1S_0}$(rose bengal) $\approx 14{,}700\,\mathrm{cm}^{-1}$ [47], and $\tilde{\nu}_{T_1S_0}(C_{70}) \approx 12{,}400$–$12{,}900\,\mathrm{cm}^{-1}$ [48–50].

In the ground-state absorption region where the singlet absorption cross-section, σ_a, is larger than the triplet absorption cross-section, σ_T, the triplet–triplet absorption cross-sections depend critically on the quantum yield of triplet formation, σ_T. If a ϕ_T-value is used in the calculations which is smaller than the real ϕ_T-value, then the calculated probe pulse ground-state transmission may become as small or smaller than the measured probe pulse transmission resulting in apparent zero or negative triplet absorption cross-section. Assuming a smooth continuation of the triplet-absorption cross-section spectra through the strong S_0–S_1 absorption cross-section region allows an accurate determination of ϕ_T. For the samples studied here we got best results using $\phi_T \approx 1-\phi_F$ (see Table 1). For eosin Y in methanol a value of $\phi_T = 0.56$ was reported previously [38] in agreement with the relation $\phi_T \approx 1-\phi_F$ ($\phi_F \approx 0.44$) [38]). For erythrosin B the fluorescence quantum yield is $\phi_F = \tau_F/\tau_{rad} \approx 0.1$ ($\tau_F \approx 530$ ps [51], $\tau_{rad} \approx 5$ ns, τ_{rad} is given by the relation [52,53] $\tau_{rad}^{-1} = 8\pi c_0 \left[\int_{S_1-S_0} E_F(\lambda)\mathrm{d}\lambda / \int_{S_1-S_0} E_F(\lambda)\lambda^3 n^{-3}(\lambda)\mathrm{d}\lambda\right] \int_{S_1-S_0} \sigma_a(\lambda)\lambda^{-1} n^{-1}(\lambda)\mathrm{d}\lambda$ where $E_F(\lambda)$ is the fluorescence quantum distribution and $n(\lambda)$ the refractive index). A value of ϕ_T (erythrosin B/methanol) = 0.94 was reported in [54]. For rose bengal the fluorescence quantum yield is $\phi_F = \tau_F/\tau_{rad} \approx 0.1$ ($\tau_F \approx 590$ ps [51], $\tau_{rad} = 5.8$ ns [55]). A value of $\phi_T = 0.86$ was reported in [56] and a value of $\phi_T = 0.96$ was reported in [57]. For C_{70} in toluene it is $\phi_F \approx 8.5 \times 10^{-4}$ [23,36] and $\phi_T \approx 1$ [22,36,58]. The quantum yields of triplet formation determined in [51] by a picosecond laser double-pulse fluorescence excitation technique seem to be too small, probably because of incorrect overlap of the pump and probe pulses.

In the Figs. 11–14 previously reported triplet–triplet absorption cross-section spectra are included. For eosin Y in methanol (Fig. 11) the triplet–triplet absorption cross-section spectrum determined in [15] agrees reasonably well with the present spectrum for $\lambda > 600$ nm. Around the S_0–S_1 absorption maximum a somewhat larger triplet–triplet absorption cross-section spectrum is calculated in the present work. In the short wavelength region (<470 nm) larger absorption cross-sections were obtained previously. In the previous experiment, the sample was excited with XeCl excimer laser pump pulses ($\lambda_P = 308$ nm, $\Delta t_P \approx 10$ ns) and probed with picosecond light continua at a temporal delay of $t_d = (750 \pm 150)$ ns. Within the delay time some transient photoproducts may have been formed causing a modified absorption [41,59]. The applied UV excimer laser excitation probably caused a stronger photodegradation than the present picosecond visible laser excitation.

For erythrosin B in gelatin a triplet–triplet absorption cross-section spectrum was determined by microsecond flash photolysis in the wavelength region from 420 to 670 nm [17] (dotted curve in Fig. 12). Outside the S_0–S_1 absorption peak region the agreement with our measurements

is good. A slight increase of the triplet population in the data fit of [17] would also lead to a good agreement with our data in the absorption region [17]. A triplet absorption cross-section for erythrosin B in water (pH 9) at 526 nm reported by [16] (diamond in Fig. 12) lies somewhat higher than our result. An accurate determination of σ_T at this wavelength in the absorption peak region is difficult because small changes in the residual ground-state population have a strong influence on the apparent value of σ_T.

For rose bengal in 5×10^{-3} molar phosphate-buffered saline a triplet–triplet absorption cross-section spectrum was determined in the wavelength region from 480 to 590 nm (dotted curve in Fig. 13) by nanosecond frequency doubled Nd : YAG laser pump pulse excitation and xenon arc lamp probing [18]. In the region of peak S_0–S_1 absorption a rather large triplet–triplet absorption was obtained. In this wavelength region, our σ_T values are smaller. Slight reductions of triplet-population in [18] would reduce the triplet–triplet absorption to our results.

For C_{70} in benzene the triplet–triplet absorption cross-section spectra have been measured by several groups [19–23]. The reported results are included in Fig. 14. All the absorption spectra agree within a factor of two.

7. Conclusions

The triplet–triplet absorption cross-section spectra of the xanthene dyes eosin Y, erythrosin B, and rose bengal and of the fullerene C_{70} have been determined over a wide wavelength region from 390 to 1600 nm by a picosecond laser photolysis technique using intensive picosecond excitation pulses and nanosecond time-delayed picosecond probe pulse continua. Reasonably accurate triplet–triplet absorption cross-section spectra could be determined. In the wavelength region of strong S_0–S_1 absorption the sensitive dependence of σ_T on the quantum yield of triplet formation, σ_T could be used to determine ϕ_T rather accurately.

The applied technique of picosecond laser excitation and nanosecond delayed picosecond light continuum probing avoids spectral influences by transient photoproducts which may be formed on a longer time scale within the microsecond to millisecond triplet system lifetime.

The technique of picosecond pulse excitation additionally avoids complications of dynamics description and data analysis by pump-pulse induced triplet–singlet back intersystem crossing when the pump pulse durations become comparable to or longer than the fluorescence lifetime (considerable triplet state population during pump pulse duration) [25–27].

A knowledge of the triplet–triplet absorption cross-section spectra of molecules is important for quantitative studies of photo-induced effects by excited triplet molecules in the fields of photophysics, photochemistry, photobiology and photomedicine.

Acknowledgements

The authors thank the Deutsche Forschungsgemeinschaft for financial support and the Rechenzentrum of the University of Regensburg for allocation of computer time.

References

[1] C.A. Parker, in: A.B. Zahlan (Ed.), The Triplet State, Cambridge University Press, Cambridge, 1967, p. 372.
[2] C.A. Parker, Photoluminescence of Solutions, Elsevier, Amsterdam, 1968.
[3] J.B. Birks, Photophysics of Aromatic Molecules, Wiley-Interscience, London, 1970.
[4] M.S. Dresselhaus, G. Dresselhaus, P.C. Eklund, Science of Fullerenes and Carbon Nanotubes, Academic Press, San Diego, 1996.
[5] I. Carmichael, G.I. Hug, J. Phys. Chem. Ref. Data 15 (1986) 1.
[6] I. Carmichael, G.I. Hug, J. Phys. Chem. Ref. Data 16 (1987) 239.
[7] I. Carmichael, G.I. Hug, in: J.C. Scaiano (Ed.), Handbook of Organic Photochemistry, vol. 1, CRC Press, Boca Raton, 1989, p. 369.
[8] E. Thiel, K.H. Drexhage, Chem. Phys. Lett. 199 (1992) 329.
[9] R. Astier, Y.H. Meyer, in: A.B. Zahlan (Ed.), The Triplet State, Cambridge University Press, Cambridge, 1967, p. 447.
[10] D.N. Dempster, T. Morrow, M.F. Quinn, J. Photochem. 2 (1973/74) 403.
[11] T.G. Pavlopoulos, Spectrochim. Acta A 42 (1986) 47.
[12] T.G. Pavlopoulos, SPIE. 1437 (1991) 168.
[13] T.G. Pavlopoulos, D.J. Golich, J. Appl. Phys. 67 (1990) 1203.
[14] T.G. Pavlopoulos, J.H. Boyer, K. Thangaraj, G. Sathyamoothi, M.P. Shah, M.L. Soong, Appl. Opt. 31 (1992) 7089.
[15] A. Penzkofer, A. Beidoun, Chem. Phys. 177 (1993) 203.
[16] P.G. Bowers, G. Porter, Proc. R. Soc. London Ser. A 299 (1967) 348.
[17] A.V. Buettner, J. Phys. Chem. 68 (1964) 3253.
[18] C.R. Lambert, H. Stiel, D. Leupold, M.C. Lynch, I.E. Kochevar, Photochem. Photobiol. 63 (1996) 154.
[19] R.V. Bensasson, T. Hill, C. Lambert, E.I. Land, S. Leach, T.G. Truscott, Chem. Phys. Lett. 206 (1993) 197.
[20] S. Leach, in: K. Prassides (Ed.), Physics and Chemistry of the Fullerenes, Kluwer Academic Publishers, Netherlands, 1994, p. 117.
[21] N.M. Dimitrijević, P.V. Kamat, J. Phys. Chem. 96 (1992) 4811.
[22] D.K. Palit, A.V. Sapre, J.P. Mittal, C.N.R. Rao, Chem. Phys. Lett. 195 (1992) 1.
[23] J.W. Arbogast, C.S. Foote, J. Am. Chem. Soc. 113 (1991) 8886.
[24] D. McBranch, L. Smilowitz, V. Klimov, A. Koskelo, J.M. Robinson, B.R. Mattes, J.C. Hummelen, F. Wudl, J.C. Withers, N.F. Borrelli, SPIE 2530 (1995) 196.
[25] S. Reindl, A. Penzkofer, Chem. Phys. 211 (1996) 431.
[26] N. Duran, G. Cilento, Photochem. Photobiol. 32 (1980) 113.
[27] W.G. McGimpsey, J.C. Scaiano, J. Am. Chem. Soc. 111 (1989) 335.
[28] W. Scheidler, A. Penzkofer, Opt. Commun. 80 (1990) 127.
[29] V.G. Dimitrev, G.G. Gurzadyan, D.N. Nikogosyan, Handbook of Nonlinear Optical Crystals, Springer, New York, 1991.
[30] G. Grönninger, A. Penzkofer, Opt. Quantum Electron. 85 (1984) 473.
[31] A. Penzkofer, A. Beidoun, H.J. Lehmeier, Opt. Quantum Electron. 25 (1993) 317.
[32] R.R. Alfano (Ed.), The Supercontinuum Laser Source, Springer, New York, 1984.
[33] M. Hercher, Appl. Phys. Opt. 6 (1967) 942.
[34] S. Speiser, R. van der Werf, J. Kommandeur, Chem. Phys. 1 (1973) 297.
[35] F. Henari, J. Callaghan, H. Stiel, W. Blau, D.J. Cardin, Chem. Phys. Lett. 199 (1992) 325.
[36] S. Reindl, A. Penzkofer, H. Gratz, J. Photochem. Photobiol. A: Chem. 115 (1998) 89.
[37] A. Penzkofer, W. Bäumler, Opt. Quantum Electron. 23 (1991) 439.

[38] A. Penzkofer, A. Beidoun, M. Daiber, J. Lumminesc. 51 (1992) 297.
[39] P.P. Feofilov, The Physical Basis of Polarized Emission, Consultants Bureau, New York, 1961, p. 108.
[40] M. Koizumi, Y. Usui, Mol. Photochem. 4 (1972) 57.
[41] V. Kasche, Photochem. Photobiol. 6 (1967) 643.
[42] T. Ohno, S. Kato, M. Koizumi, Bull. Chem. Soc. Jpn. 39 (1966) 232.
[43] V. Kasche, L. Lindqvist, Photochem. Photobiol. 4 (1965) 923.
[44] C.A. Parker, C.G. Hatchard, Trans. Faraday Soc. 57 (1961) 1894.
[45] R.W. Chambers, D.R. Kearns, Photochem. Photobiol. 10 (1969) 215.
[46] M. Hilbert, B. Német, Acta Physica at Chemica 24 (1978) 365.
[47] J. Paczkowski, J.J.M. Lamberts, B. Paczkowska, D.C. Neckers, J. Free Rad. Biol. Med. 1 (1985) 341.
[48] S.P. Sibley, S.M. Argentine, A.H. Francis, Chem. Phys. Lett. 188 (1992) 187.
[49] H. Ajie, M.M. Alvarez, S.J. Anz, R.D. Beck, F. Dietrich, K. Fostiropoulos, D.R. Huffman, W. Krätschmer, Y. Rubin, K.E. Schriver, D. Sensharma, R.L. Whetten, J. Phys. Chem. 94 (1990) 8630.
[50] R.E. Haufler, L.-S. Wang, L.P.F. Chibante, C.-M. Jen, J.J. Conceicao, Y. Chai, R.E. Smalley, Chem. Phys. Lett. 179 (1991) 449.
[51] S. Reindl, A. Penzkofer, Chem. Phys. 213 (1996) 429.
[52] S.J. Strickler, R.A. Berg, J. Chem. Phys. 37 (1962) 814.
[53] J.B. Birks, D.J. Dyson, Proc. R. Soc. London Ser. A 275 (1963) 135.
[54] H.E. Lessing, A. von Jena, in: M.L. Stitch (Ed.), Laser Handbook, vol. 3, North-Holland, Amsterdam, 1979, p. 753.
[55] I.B. Berlman, Handbook of Fluorescence Spectra of Aromatic Molecules, 2nd ed., Academic Press, New York, 1971, p. 415.
[56] E. Garidin, Y. Lion, A. van de Horst, Photochem. Photobiol. 37 (1983) 144.
[57] P. Murasecco-Suardi, E. Gassmann, A.M. Braun, E. Oliveros, Helv. Chem. Acta 70 (1987) 1766.
[58] R.R. Hung, J.J. Grabowski, Chem. Phys. Lett. 192 (1992) 249.
[59] J. Chrysochoos, J. Ovadia, L.F. Grossweiner, J. Phys. Chem. 71 (1967) 1629.
[60] D. von der Linde, O. Benecker, A. Laubereau, Opt. Commun. 2 (1970) 215.
[61] A. Penzkofer, W. Falkenstein, W. Kaiser, Chem. Phys. Lett. 44 (1976) 82.
[62] G.R. Fleming, J.M. Morris, G.W. Robinson, Chem. Phys. 17 (1976) 91.
[63] F. Graf, A. Penzkofer, Opt. Quantum Electron. 17 (1989) 53.
[64] R.C. West (Ed.), CRC Handbook of Chemistry and Physics, 1st Student ed., CRC Press, Boca Raton, FL, 1987, p. F-23.